Kinetic-thermodynamic model for carbon incorporation during step-flow growth of GaN by metalorganic vapor phase epitaxy

Y. Inatomi,[1,*] Y. Kangawa,[1,2,3] A. Pimpinelli,[4] and T. L. Einstein[5]

[1]*Department of Aeronautics and Astronautics, Kyushu University, Fukuoka 819-0395, Japan*

[2]*Research Institute for Applied Mechanics (RIAM), Kyushu University, Fukuoka 816-8580, Japan*

[3]*Institute of Materials and Systems for Sustainability (IMaSS), Nagoya University, Nagoya 464-8601, Japan*

[4]*Smalley-Curl Institute, Rice University, Houston, Texas 77005-1892, USA*

[5]*Department of Physics, University of Maryland, College Park, Maryland 20742-4111, USA*

(Received 23 August 2018; published 2 January 2019)

Relationships between concentration of unintentionally doped carbon in GaN and its metalorganic vapor phase epitaxy conditions were investigated theoretically. A kinetic-thermodynamic model which considers kinetic behavior of adsorbed atoms on vicinal surface was proposed. Thermodynamic properties of gas species and adsorption energies obtained by first-principles calculation were used in the model. The predicted carbon concentration range, $10^{15} \sim 10^{17}$ cm^{-3}, agreed with that of experimental results quantitatively. The calculation results also reproduced experimental tendency: Carbon concentration decreases with increase of NH_3 partial pressure and total pressure and/or decrease of trimethylgallium partial pressure.

DOI: 10.1103/PhysRevMaterials.3.013401

I. INTRODUCTION

Electronic devices composed of gallium nitride (GaN) have attracted much attention due to GaN's excellent properties, such as high electron saturation velocity, high breakdown field, and wide band gap. Recently, researchers have been focusing on the development of high-voltage/high-current vertical GaN power devices for application to hybrid and electric vehicles [1–5]. To fabricate the vertical GaN power devices with high breakdown voltage over 1 kV, the carrier concentration in the drift layer must be reduced below 10^{16} cm^{-3} [6]. That is, high-purity GaN with few contaminations is necessary to make a low-carrier-concentration and low-resistive-drift layer since carbon atoms will compensate Si donors as deep acceptors. It is known, however, that $\sim 10^{16}$ cm^{-3} of carbon atoms are incorporated in GaN layers grown by conventional metalorganic vapor phase epitaxy (MOVPE). The carbon atoms mainly come from trimethylgallium (TMG), the Ga source. Reducing carbon concentration in the GaN drift layer is crucial to develop high-voltage electronic devices.

Experiments have been performed to study the relationships between carbon concentration in GaN layers and their growth conditions such as growth temperature, total pressure, V/III ratio, and carrier gas species [7–16]. Many researchers reported that carbon concentration decreases with increasing NH_3 partial pressure [7,8,12–16], while high TMG flow rate increases carbon concentration in GaN layers [7,8,11,13,14]. In general, the growth rate increases linearly with the TMG flow rate because conventional MOVPE is performed at a high V/III ratio, more than 1000. Therefore, the observed increase of the carbon concentration implies that the carbon incorporation rate increases faster than the growth rate, since carbon concentration is simply estimated from (carbon incorporation rate)/(growth rate). On the other hand, Piao *et al.* [14] reported that carbon concentration is inversely proportional to V/III ratio, i.e., $n_{\mathrm{carbon}} \propto (\mathrm{V/III\ ratio})^{-1}$. Their results suggest that the carbon concentration could be maintained at a low value while increasing the growth rate by increasing both the NH_3 and the TMG flow rates [14]. Also, the carbon concentration was found to decrease as growth temperature and/or total pressure increase [7,8]. The carrier gas ratio, i.e., H_2/N_2 ratio, also influences the carbon concentration. The carbon concentration was found to become high when the carrier gas is H_2-rich in the case of GaN(0001) growth [7,9,10,12], although high H_2/N_2 carrier gas ratio decreases carbon impurities in case of GaN(000$\bar{1}$) growth [16]. The correlations between carbon concentration and growth conditions are summarized in Table I.

To understand and control carbon incorporation during GaN MOVPE, many theoretical studies have been performed [17–21]. Some researchers investigated the nature of carbon in GaN based on first-principles calculations [17–19]. In these studies, the formation energy of carbon-related defect in bulk GaN is calculated. The relationships between carbon concentration and growth conditions, however, were not analyzed. Reddy *et al.* [20] proposed a quantitative theoretical framework to obtain the relationship between carbon concentration and growth conditions, focusing on the chemical potential of the gaseous sources. However, these theoretical studies did not consider the role of the crystal surface, i.e., the influence of surface orientation and surface reconstruction, as well as the kinetic growth process on the surface. Kempisty *et al.* [21] investigated the formation energy of carbon substituting for nitrogen, C_N, in subsurface layers of reconstructed GaN(0001) and GaN(000$\bar{1}$). In the literature, interplanar carbon diffusion in subsurface layers was discussed as a way to understand the influence of surface reconstruction on carbon incorporation.

*inatomi@riam.kyushu-u.ac.jp

TABLE I. Summary of reported correlations between carbon concentration and growth conditions.

Growth condition	NH_3 ▲	TMG ▲	H_2/N_2 ▲	p_{total} ▲	T ▲	Growth direction	Reference
Carbon concentration	▼	▲	▲	▼	▼	–	D.D. Koleske[7]
	▼	▲		▼	▼	[0001]	N. A. Fichtenbaum[8]
						[000$\bar{1}$]	
			▲			[0001]	T. -T. Yuan[9]
	▼		▲			[0001]	J. Zhang[10]
		▲				[0001]	Q. Mao[11]
	▼		▲			[0001]	F. Kaess[12]
	▼	▲				[0001]	W. V. Lundin[13]
	▼	▲				[0001]	G. Piao[14]
	▼	▲				[1$\bar{1}$00]	O. I. Barry[15]
	▼		▼			[000$\bar{1}$]	T. Tanikawa[16]

▲: increase, ▼: decrease

In the present paper, we propose a kinetic-thermodynamic model of impurity incorporation which considers the kinetic growth process on a growing surface and the role of the surface orientation. Furthermore, the relationships between carbon concentration and growth conditions in GaN(0001) MOVPE are discussed using this theoretical model.

II. CALCULATION METHOD

When a crystal grows from the gas phase, the net flux of particles both from gas phase to adsorbed phase and from adsorbed phase to crystal are positive. Therefore, the chemical potential of each system satisfies the following relation:

$$\mu_{\text{solid}} < \mu_{\text{ad}} < \mu_{\text{gas}}. \tag{1}$$

However, if the adsorption-desorption process between gas phase and adsorbed phase is assumed to be sufficiently fast with respect to the process of incorporation of adatoms into crystal, i.e., adsorbed particles→crystal is the rate-determining step, then the chemical potentials satisfy the relation

$$\mu_{\text{solid}} \ll \mu_{\text{ad}} \cong \mu_{\text{gas}}. \tag{2}$$

In the present model, we assume that the chemical potentials of adsorbed phase and gas phase are equal during crystal growth:

$$\mu_{\text{ad}} = \mu_{\text{gas}}. \tag{3}$$

First, we considered adsorbed particles based on statistical thermodynamics. The thermodynamic properties of typical gases and solids are well known, while those of adsorbed particles are unknown in principle. In order to evaluate the thermodynamic properties of adsorbed particles, they are taken to be a two-dimensional (2D) gas constrained on top of the crystal surface; in other words, as N particles in a 2D box of size $(l_x \times l_y)$. Using quantum statistical mechanics, the canonical partition function Q of this system is expressed as

$$Q_{\text{2D}} = \frac{(q_{\text{2D-trans}} \cdot q_{\text{2D-other}})^N}{N!} = \frac{1}{N!}\left(\frac{l_x l_y}{\Lambda^2} q_{\text{2D-other}}\right)^N. \tag{4}$$

Here, $q_{\text{2D-trans}} = (l_x l_y/\Lambda^2)$ is the partition function of 2D translational motion, $q_{\text{2D-other}}$ is the partition function of internal degrees of freedom other than translations such as rotations and vibrations, $\Lambda = h/\sqrt{2\pi mkT}$ is the thermal de Broglie wavelength, h is Planck's constant, m is the mass of each particle, k is Boltzmann's constant, and T is the temperature. Using the statistical thermodynamic definition of free energy $A(T) - A(0) = -kT \ln Q$, and inserting Eq. (4), the Helmholtz energy of this system can be written as

$$\begin{aligned} A_{\text{2D}}(T) &= -kT \ln Q_{\text{2D}} - Nu \\ &\cong N\left[kT \ln\left(\frac{N\Lambda^2}{l_x l_y q_{\text{2D-other}}}\right) - kT - u\right], \end{aligned} \tag{5}$$

where u denotes the particle's surface potential relative to the gas phase, i.e., the adsorption energy. The Stirling formula $[\ln N \cong N(\ln N - 1)]$ was used for the transformation from the second line to the third line of Eq. (5). Then, the chemical potential of the particle was derived by partial differentiation of Eq. (5):

$$\begin{aligned} \mu_{\text{ad}} &= \left(\frac{\partial A_{\text{2D}}}{\partial N}\right)_T = kT \ln \frac{\Lambda^2 \rho_{\text{ad}}}{q_{\text{2D-other}}} - u \\ &= kT \ln \frac{\rho_{\text{ad}} h^2}{2\pi mkT q_{\text{2D-other}}} - u, \end{aligned} \tag{6}$$

where $\rho_{\text{ad}} = (N/l_x l_y)$ is surface density of the particles (atoms/m^2). By inverting Eq. (6), we get surface density of

the particles as a function of their chemical potential:

$$\rho_{\rm ad} = \frac{2\pi mkT}{h^2} \exp\left(\frac{\mu_{\rm ad} + u}{kT}\right). \tag{7}$$

Assuming adsorbed phase–gas phase equilibrium, we use Eq. (3) to replace $\mu_{\rm ad}$ by $\mu_{\rm gas}$ Eq. (7); then $\rho_{\rm ad}$ can be computed as a function of the chemical potential of the gas near the crystal surface.

Next, following standard gas molecular-kinetics techniques, we derive surface flux of adsorbed particles, considering 2D crystal surface where there is a line of width D perpendicular to the x axis. The particles which have velocity $v_x(>0)$ and are present in the area of $Dv_x\Delta t$ collide with the line during Δt s. Since the average number of the particles existing in the unit area of the crystal surface is $\rho_{\rm ad}$, the total number of collision during Δt is given by $\rho Dv_x\Delta t$. Moreover, we must consider the range of velocities of the particles. Like an ideal gas (three-dimensional free particles), the 2D free particles also follow the Maxwell distribution: $f_x = \sqrt{m/2\pi kT}\exp(-mv_x^2/2kT)$. Therefore, the total number of collisions in the interval Δt is expressed as

$$\begin{aligned}\text{Number of collisions} &= \int_0^\infty (Dv_x\Delta t \cdot \rho_{\rm ad}) f_x dv_x \\ &= D\Delta t\rho_{\rm ad}\sqrt{\frac{kT}{2\pi m}},\end{aligned} \tag{8}$$

where Gaussian integral formula $\int_0^\infty xe^{-C_0x^2} = 1/(2C_0)$ was used. Dividing the number of collisions by the linewidth D and Δt leads to the collision flux.

$$\begin{aligned}J_{\rm ad} &= \frac{\text{Number of collisions}}{D\Delta t} = \sqrt{\frac{kT}{2\pi m}}\rho_{\rm ad} \\ &= \frac{\sqrt{2\pi m(kT)^3}}{h^2}\exp\left(\frac{\mu_{\rm ad}+u}{kT}\right),\end{aligned} \tag{9}$$

where Eq. (7) was used. Assuming adsorbed phase–gas phase equilibrium and substituting Eq. (3) into Eq. (9), the surface flux of the particles can also be calculated as a function of the chemical potential of the gas near the crystal surface.

Figure 1 shows a schematic of a GaN(0001) surface during step flow growth. There are two types of step edges, Ga-exposed step edge and N-exposed step edge. We call the total length of Ga- and of N-exposed step edge per unit area of growing surface $L_{\rm Ga}$ and $L_{\rm N}$, respectively. In step flow growth, particles impinge on the surface, then either desorb or reach steps, where they are incorporated into the crystal at kinks. Here, we assumed that growth of the crystal is limited by the impingement flux of the gas particles onto steps as given by Eq. (9). Furthermore, we assumed that adsorbed Ga atoms are incorporated into the crystal only when they impinge on the N-exposed edge. Similarly, adsorbed N atoms are incorporated only when they impinge on the Ga-exposed edge. Since carbon atoms have similar atomic features to nitrogen and substitute for nitrogen in GaN, adsorbed carbon atoms are also incorporated by impinging on the Ga-exposed edge. Then, for each species the incorporation rate (number of incorporated atoms per unit area and per unit time) is

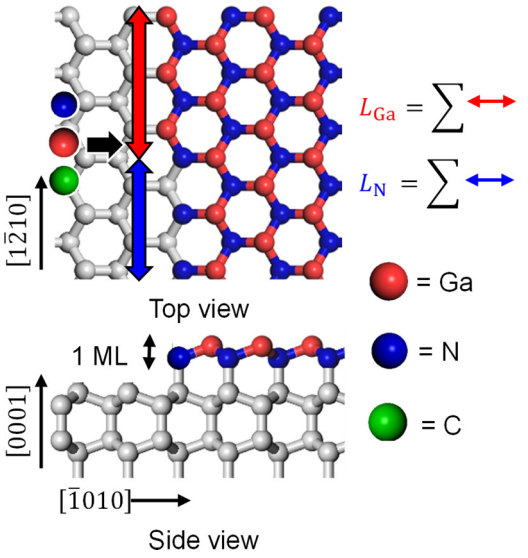

FIG. 1. Schematic of growing surface of GaN(0001).

expressed as follows:

$$\begin{aligned}&\text{Incorporation rate of Ga} : L_N J_{Ga} \\ &\text{Incorporation rate of N} : L_{Ga} J_N \\ &\text{Incorporation rate of C} : L_{Ga} J_C\end{aligned} \tag{10}$$

Here, $J_{\rm N}$ is defined as the total N flux including the flux of NH_x molecules.

When N atoms are incorporated along a segment of Ga-exposed step of length $L_{\rm Ga}$, that step segment becomes N-exposed step. When Ga atoms desorb from a segment of Ga-exposed step of length $L_{\rm Ga}$, the step segment also converts into N-exposed step. Therefore, the rate of increase of $L_{\rm N}$ is expressed as

$$\left(\frac{dL_{\rm N}}{dt}\right)_{\rm increase} \propto L_{\rm Ga}\left(J_{\rm N} + J^d_{\rm Ga}\right), \tag{11}$$

where we defined J^d_i as desorption flux of the ith type of atom (Ga or N) from an ith atom exposed step. On the other hand, N-exposed step changes to Ga-exposed step when Ga atoms are incorporated into N-exposed step, and N atoms desorb from N-exposed step. Therefore, the rate of decrease of $L_{\rm N}$ is expressed as

$$\left(\frac{dL_{\rm N}}{dt}\right)_{\rm decrease} \propto -L_{\rm N}\left(J_{\rm Ga} + J^d_{\rm N}\right). \tag{12}$$

Since $L_{\rm N}$ does not change with time, i.e., $(\frac{dL_{\rm N}}{dt})_{\rm increase} = -(\frac{dL_{\rm N}}{dt})_{\rm decrease}$, thus in steady state, Eqs. (11) and (12) imply

$$\frac{L_{\rm Ga}}{L_{\rm N}} = \frac{J_{\rm Ga} + J^d_{\rm N}}{J_{\rm N} + J^d_{\rm Ga}}. \tag{13}$$

Since the number of Ga atoms incorporated into N-exposed step edge and desorbing from Ga-exposed step edge on the growing surface (per unit area per unit time) are expressed as $L_{\rm N}J_{\rm Ga}$ and $L_{\rm Ga}J^d_{\rm Ga}$, respectively, the net incorporation rate of Ga atoms $V_{\rm Ga}$ is

$$V_{\rm Ga} = L_{\rm N}J_{\rm Ga} - L_{\rm Ga}J^d_{\rm Ga}. \tag{14}$$

Similarly, the net incorporation rate of N atoms V_{N} is

$$V_{\mathrm{N}} = L_{\mathrm{Ga}} J_{\mathrm{N}} - L_{\mathrm{N}} J_{\mathrm{N}}^{d}. \tag{15}$$

Therefore, the growth rate of GaN V_{GaN} (pair/s) takes the form

$$\begin{aligned} V_{\mathrm{GaN}} =& \frac{1}{2}\{V_{\mathrm{Ga}} + V_{\mathrm{N}}\} = \frac{1}{2}\left\{\left(L_{\mathrm{N}} J_{\mathrm{Ga}} - L_{\mathrm{Ga}} J_{\mathrm{Ga}}^{d}\right) + \left(L_{\mathrm{Ga}} J_{\mathrm{N}} - L_{\mathrm{N}} J_{\mathrm{N}}^{d}\right)\right\} = \frac{L_{\mathrm{Ga}} + L_{\mathrm{N}}}{2} \times \frac{L_{\mathrm{G}}\left(J_{\mathrm{N}} - J_{\mathrm{Ga}}^{d}\right) + L_{\mathrm{N}}\left(J_{\mathrm{Ga}} - J_{\mathrm{N}}^{d}\right)}{L_{\mathrm{Ga}} + L_{\mathrm{N}}} \\ =& \frac{L_{\mathrm{Ga}} + L_{\mathrm{N}}}{2} \frac{\left(J_{\mathrm{Ga}} + J_{\mathrm{N}}^{d}\right)\left(J_{\mathrm{N}} - J_{\mathrm{Ga}}^{d}\right) + \left(J_{\mathrm{N}} + J_{\mathrm{Ga}}^{d}\right)\left(J_{\mathrm{Ga}} - J_{\mathrm{N}}^{d}\right)}{J_{\mathrm{Ga}} + J_{\mathrm{N}} + J_{\mathrm{Ga}}^{d} + J_{\mathrm{N}}^{d}} = (L_{\mathrm{Ga}} + L_{\mathrm{N}}) \frac{J_{\mathrm{Ga}} J_{\mathrm{N}} - J_{\mathrm{Ga}}^{d} J_{\mathrm{N}}^{d}}{J_{\mathrm{Ga}} + J_{\mathrm{N}} + J_{\mathrm{Ga}}^{d} + J_{\mathrm{N}}^{d}}, \end{aligned} \tag{16}$$

where Eq. (13) was used. Defining the C concentration n_{C} in a GaN crystal as $n_C = V_C / V_{\mathrm{GaN}}$, where $V_C = L_{\mathrm{Ga}} J_C$ is the C incorporation rate at Ga-exposed step edges, we can write

$$\begin{aligned} n_{\mathrm{C}} =& \frac{L_{\mathrm{Ga}} J_{\mathrm{C}}}{\frac{1}{2}\left\{\left(L_{\mathrm{N}} J_{\mathrm{Ga}} - L_{\mathrm{Ga}} J_{\mathrm{Ga}}^{d}\right) + \left(L_{\mathrm{Ga}} J_{\mathrm{N}} - L_{\mathrm{N}} J_{\mathrm{N}}^{d}\right)\right\}} = \frac{2 L_{\mathrm{Ga}} J_{\mathrm{C}}}{L_G\left(J_{\mathrm{N}} - J_{\mathrm{Ga}}^{d}\right) + L_N\left(J_{\mathrm{Ga}} - \mathrm{J}_{\mathrm{N}}^{\mathrm{d}}\right)} \\ =& \frac{2\left(J_{\mathrm{Ga}} + J_{\mathrm{N}}^{d}\right) J_C}{\left(J_{\mathrm{Ga}} + J_{\mathrm{N}}^{d}\right)\left(J_{\mathrm{N}} - J_{\mathrm{Ga}}^{d}\right) + \left(J_{\mathrm{N}} + J_{\mathrm{Ga}}^{d}\right)\left(J_{\mathrm{Ga}} - J_{\mathrm{N}}^{d}\right)} = \frac{\left(J_{\mathrm{Ga}} + J_{\mathrm{N}}^{d}\right) J_{\mathrm{C}}}{J_{\mathrm{Ga}} J_{\mathrm{N}} - J_{\mathrm{Ga}}^{d} J_{\mathrm{N}}^{d}}, \end{aligned} \tag{17}$$

where again Eq. (13) was used.

In this study, GaN(0001) growth by MOVPE is considered. In an MOVPE furnace, six gas species are present: Ga, N_2, H_2, NH_3, CH_4, and TMG. The following chemical equilibrium conditions between gas phase–adsorbed phase near the crystal surface are assumed. Regarding the adsorption structure of NH_x molecules, we considered the complex adsorption structures of NH_x molecules and H atom which satisfy the electron counting rule (ECR) [22] on a (2×2) surface. We could not find stable adsorption structure of NH_2.

$$\mathrm{Ga(gas)} \leftrightarrow \mathrm{Ga(ad)}, \tag{18}$$

$$\mathrm{NH_3(gas)} \leftrightarrow \mathrm{N(ad)} + \tfrac{3}{2}\mathrm{H_2(gas)}, \tag{19}$$

$$\mathrm{NH_3(gas)} \leftrightarrow \mathrm{NH(ad)} + \mathrm{H(ad)} + \tfrac{1}{2}\mathrm{H_2(gas)}, \tag{20}$$

$$\mathrm{NH_3(gas)} + \tfrac{3}{2}\mathrm{H_2(gas)} \leftrightarrow \mathrm{NH_3(ad)} + 3\mathrm{H(ad)}, \tag{21}$$

$$\mathrm{CH_4(gas)} \leftrightarrow \mathrm{C(ad)} + 2\mathrm{H_2(gas)}. \tag{22}$$

Rewriting Eqs. (18)–(22) in terms of the chemical potentials, they become

$$\mu_{\mathrm{Ga(ad)}} = \mu_{\mathrm{Ga(gas)}} = \mu^{*}_{\mathrm{Ga(gas)}} + kT \ln \frac{p_{\mathrm{Ga(gas)}}}{p^{*}}, \tag{23}$$

$$\mu_{\mathrm{N(ad)}} = \mu_{\mathrm{NH_3(gas)}} - \frac{3}{2}\mu_{\mathrm{H_2(gas)}} = \mu^{*}_{\mathrm{NH_3(gas)}} - \frac{3}{2}\mu^{*}_{\mathrm{H_2(gas)}} + kT \ln \left\{\left(\frac{p_{\mathrm{NH_3(gas)}}}{p^{*}}\right)\left(\frac{p_{\mathrm{H_2(gas)}}}{p^{*}}\right)^{-\left(\frac{3}{2}\right)}\right\}, \tag{24}$$

$$\mu_{\mathrm{NH(ad)+H(ad)}} = \mu_{\mathrm{NH_3(gas)}} - \frac{1}{2}\mu_{\mathrm{H_2(gas)}} = \mu^{*}_{\mathrm{NH_3(gas)}} - \frac{1}{2}\mu^{*}_{\mathrm{H_2(gas)}} + kT \ln \left\{\left(\frac{p_{\mathrm{NH_3(gas)}}}{p^{*}}\right)\left(\frac{p_{\mathrm{H_2(gas)}}}{p^{*}}\right)^{-\left(\frac{1}{2}\right)}\right\}, \tag{25}$$

$$\mu_{\mathrm{NH3(ad)+3H(ad)}} = \mu_{\mathrm{NH_3(gas)}} + \frac{3}{2}\mu_{\mathrm{H_2(gas)}} = \mu^{*}_{\mathrm{NH_3(gas)}} + \frac{3}{2}\mu^{*}_{\mathrm{H_2(gas)}} + kT \ln \left\{\left(\frac{p_{\mathrm{NH_3(gas)}}}{p^{*}}\right)\left(\frac{p_{\mathrm{H_2(gas)}}}{p^{*}}\right)^{\frac{3}{2}}\right\}, \tag{26}$$

$$\mu_{\mathrm{C(ad)}} = \mu_{\mathrm{CH_4(gas)}} - 2\mu_{\mathrm{H_2(gas)}} = \mu^{*}_{\mathrm{CH_4(gas)}} - 2\mu^{*}_{\mathrm{H_2(gas)}} + kT \ln \left\{\left(\frac{p_{\mathrm{CH_4(gas)}}}{p^{*}}\right)\left(\frac{p_{\mathrm{H_2(gas)}}}{p^{*}}\right)^{-2}\right\}, \tag{27}$$

where p_i is partial pressure of the ith species near the crystal surface, p^* is the standard pressure (1.013×10^5 Pa), and μ_i^* is the chemical potential at standard pressure and the temperature of interest of ith species. We used the thermodynamic formula for an ideal gas: $\mu(p, T) = \mu^*(p^*, T) + kT \ln p/p^*$. The density of each adatom can be calculated by using Eq. (7), and their surface flux can be calculated from Eq. (9). The rotation and the vibration of the N–H bond of NH_x admolecules are ignored in

this calculation. After substituting Eqs. (23)–(27) into Eq. (9), the surface flux of each atom can be expressed as

$$J_{\mathrm{Ga(ad)}} = \frac{\sqrt{2\pi m_{\mathrm{Ga}}(kT)^3}}{h^2}\left(\frac{p_{\mathrm{Ga(gas)}}}{p^*}\right)e^{\frac{\mu^*_{\mathrm{Ga(gas)}}+u_{\mathrm{Ga(ad)}}}{kT}}, \tag{28}$$

$$J_{\mathrm{N(ad)}} = \frac{\sqrt{2\pi m_{\mathrm{N}}(kT)^3}}{h^2}\left(\frac{p_{\mathrm{NH_3(gas)}}}{p^*}\right)\left(\frac{p_{\mathrm{H_2(gas)}}}{p^*}\right)^{-\left(\frac{3}{2}\right)}e^{\frac{\mu^*_{\mathrm{NH_3(gas)}}-\left(\frac{3}{2}\right)\mu^*_{\mathrm{H_2(gas)}}+u_{\mathrm{N(ad)}}}{kT}}, \tag{29}$$

$$J_{\mathrm{NH(ad)}} = \frac{\sqrt{2\pi m_{\mathrm{N}}(kT)^3}}{h^2}\left(\frac{p_{\mathrm{NH_3(gas)}}}{p^*}\right)\left(\frac{p_{\mathrm{H_2(gas)}}}{p^*}\right)^{-\left(\frac{1}{2}\right)}e^{\frac{\mu^*_{\mathrm{NH_3(gas)}}-\left(\frac{1}{2}\right)\mu^*_{\mathrm{H_2(gas)}}+u_{\mathrm{N(ad)+H(ad)}}}{kT}}, \tag{30}$$

$$J_{\mathrm{NH3(ad)}} = \frac{\sqrt{2\pi m_{\mathrm{N}}(kT)^3}}{h^2}\left(\frac{p_{\mathrm{NH_3(gas)}}}{p^*}\right)\left(\frac{p_{\mathrm{H_2(gas)}}}{p^*}\right)^{\frac{3}{2}}e^{\frac{\mu^*_{\mathrm{NH_3(gas)}}+\left(\frac{3}{2}\right)\mu^*_{\mathrm{H_2(gas)}}+u_{\mathrm{NH3(ad)+3H(ad)}}}{kT}}, \tag{31}$$

$$J_{\mathrm{C(ad)}} = \frac{\sqrt{2\pi m_{\mathrm{C}}(kT)^3}}{h^2}\left(\frac{p_{\mathrm{CH_4(gas)}}}{p^*}\right)\left(\frac{p_{\mathrm{H_2(gas)}}}{p^*}\right)^{-2}e^{\frac{\mu^*_{\mathrm{CH_4(gas)}}-2\mu^*_{\mathrm{H_2(gas)}}+u_{\mathrm{C(ad)}}}{kT}}. \tag{32}$$

Here, we have to estimate the value of desorption flux from a step edge J_i^d. Suppose the following chemical equilibrium is established:

$$\mathrm{Ga(ad)} + \mathrm{N(ad)} \leftrightarrow \mathrm{GaN(solid)}\ or \tag{33}$$

$$\mu_{\mathrm{Ga(ad)}} + \mu_{\mathrm{N(ad)}} = \mu_{\mathrm{GaN(solid)}}. \tag{34}$$

Then, the growth rate described by Eq. (16) should be zero. Therefore, we obtain the following relationship:

$$\begin{aligned} J^d_{\mathrm{Ga}}J^d_{\mathrm{N}} &= (J_{\mathrm{Ga(ad)}}J_{\mathrm{N(ad)}})^{eqm} = \frac{2\pi(kT)^3\sqrt{m_{\mathrm{Ga}}m_{\mathrm{N}}}}{h^4}\exp\left(\frac{\mu_{\mathrm{Ga(ad)}}+\mu_{\mathrm{N(ad)}}+u_{\mathrm{Ga(ad)}}+u_{\mathrm{N(ad)}}}{kT}\right) \\ &= \frac{2\pi(kT)^3\sqrt{m_{\mathrm{Ga}}m_{\mathrm{N}}}}{h^4}\exp\left(\frac{\mu_{\mathrm{GaN(solid)}}+u_{\mathrm{Ga(ad)}}+u_{\mathrm{N(ad)}}}{kT}\right), \end{aligned} \tag{35}$$

where Eqs. (9) and (34) were used. Assuming that $J^d_{\mathrm{Ga}} = J^d_{\mathrm{N}}$, we obtain

$$J^d_{\mathrm{Ga}} = J^d_{\mathrm{N}} = \frac{\sqrt{2\pi(kT)^3}(m_{\mathrm{Ga}}m_{\mathrm{N}})^{1/4}}{h^2}\exp\left(\frac{\mu_{\mathrm{GaN(solid)}}+u_{\mathrm{Ga(ad)}}+u_{\mathrm{N(ad)}}}{2kT}\right). \tag{36}$$

We obtained the experimental values of each μ_i^* from Barin [23].

The adsorption energy of each atom u_i on a GaN(0001) surface was computed by first-principles methods. In the calculations, all electrons were treated using the DMOL [3] package [24,25] based on the density-functional theory with the Perdew-Burke-Ernzerhof functional [26], and the double numerical plus polarization basis set. A surface slab model comprised a vacuum layer of more than 20 Å and five GaN bilayers. The bottom layer was fixed and passivated with fictitious hydrogen atoms and was used for a surface system [27]. A $3 \times 3 \times 1$ Monkhorst-Pack k-point mesh was used for the (2×2) surface slab models of GaN(0001). The geometry-optimization convergence thresholds were 10^{-5} Ha for energy change, 2.0×10^{-3} Ha/Å for maximum force, and 5.0×10^{-3} Å for maximum displacement. The validity of these calculational settings has been confirmed by our previous study [28,29]. The results show that the Ga adatom prefers the hexagonal close-packed (hcp) site and has an adsorption energy of 3.66 eV at this position. The adsorption energy of Ga on the fcc site has a slightly lower value, 3.42 eV. This is because the Ga adatom on the hcp site is attracted by the N atom of the layer below. Correspondingly, the N adatom prefers the fcc site (5.89 eV) and is relatively unstable on the hcp site (3.82 eV); the N adatom on the hcp site is repelled by the N atom of the layer below. The NH molecule prefers the fcc site and makes bonds with three Ga on the surface first layer. In order to satisfy ECR [22], H is adsorbed on the remaining surface Ga. The adsorption energy of this structure is 13.28 eV. The NH_3 molecule is stable on the top site and the remaining three Ga are bonded to H to satisfy ECR. The adsorption energy of this structure is 25.24 eV. For the C adatom, the adsorption energies on the fcc site and hcp site are almost the same, 5.88 eV (fcc) and 5.89 eV (hcp), because C is neutral. Each of Ga, N, NH, and C on the top site is unstable. In this study, we used the values u at the favored binding sites: $u_{\mathrm{Ga(ad)}} = 3.66$ eV (hcp), $u_{\mathrm{N(ad)}} = 5.89$ eV (fcc), $u_{\mathrm{NH(ad)+3H(ad)}} = 13.28$ eV (fcc for NH and top for H), $u_{\mathrm{NH3(ad)+3H(ad)}} = 25.24$ eV (top for NH_3 and H), and $u_{\mathrm{C}} = 5.89$ eV (hcp). Figure 2 shows the geometry-optimized structure of the GaN(0001) surface slab model with each atom adsorbed at the most stable sites.

Now we describe the gas phase conditions in the growth furnace. We denote the mole fraction of each gas species near the crystal surface as y_i, and denote the mole fraction and partial pressure in the gas flowing through the inlet as y_i^0 and p_i^0, respectively. The supplied TMG is assumed to

completely decompose into Ga and CH_4 before reaching the crystal surface:

$$y_{\mathrm{TMG}} = 0, \tag{37}$$

$$y_{\mathrm{CH_4}} = 3y^0_{\mathrm{TMG}}. \tag{38}$$

The mole fractions of Ga and NH_3, the source gases, decrease near the growth surface because they are taken into the crystal by molecular diffusion. Here, the decreasing ratio $y_{\mathrm{Ga}}/y^0_{\mathrm{TMG}}$ is thought to be small because Ga is diluted with respect to other chemical species. The ratio $y_{\mathrm{Ga}}/y^0_{\mathrm{TMG}}$ is essentially an unknown factor because it depends on growth conditions and design of the growth furnace. We introduce β as shorthand for this decreasing Ga ratio:

$$\beta = y_{\mathrm{Ga}}/y^0_{\mathrm{TMG}}. \tag{39}$$

On the other hand, the corresponding ratio for NH_3 is assumed to be 1 because typical GaN MOVPE is carried out under N-rich conditions (V/III>1000):

$$y_{\mathrm{NH_3}} = y^0_{\mathrm{NH_3}}. \tag{40}$$

The carrier gas is N_2. Since a small amount of H_2 is generated by the decomposition of NH_3, we define a parameter F as mole fraction of H_2 to ($H_2 + N_2$) in the gas near the surface.

$$y_{\mathrm{H_2}} = \left(1 - \sum_{i \neq \mathrm{H_2},\ \mathrm{N_2}} y_i\right) F, \tag{41}$$

$$y_{\mathrm{N_2}} = \left(1 - \sum_{i \neq \mathrm{H_2},\ \mathrm{N_2}} y_i\right)(1 - F). \tag{42}$$

The molar fraction and partial pressure of each chemical species has the following relationship:

$$p_i = p_{\mathrm{total}} \cdot y_i \tag{43}$$

where p_{total} is the total pressure in the growth furnace. In the following calculations, we set the growth temperature $T = 1000\,^{\circ}\mathrm{C}$ and $F = 10^{-5}$.

III. RESULT AND DISCUSSION

Figure 3 shows contours of carbon concentration when the input TMG mole fraction (y^0_{TMG}) and total pressure (p_{total}) are varied while keeping the input NH_3 mole fraction constant:

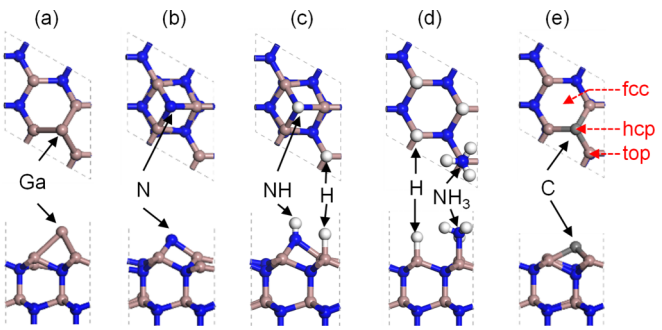

FIG. 2. Optimized structure of GaN(0001) surface on which (a) Ga[hcp], (b) N[fcc], (c) NH[fcc] + H[top], (d) NH_3[top] + 3H[top], and (e) C[hcp] atom are adsorbed.

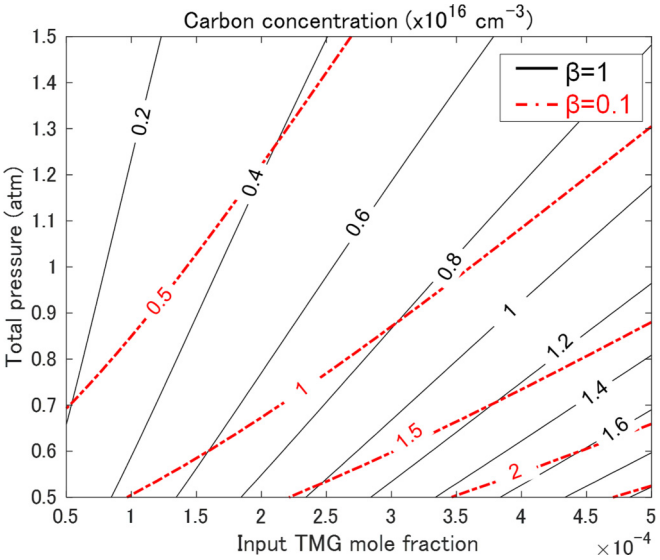

FIG. 3. Contour of carbon concentration as a function of input TMG ratio (y^0_{TMG}) and total pressure (p_{total}). $T = 1000\,^{\circ}\mathrm{C}$, $y^0_{\mathrm{NH_3}} = 0.1$, $F = 10^{-5}$. Black line and red dot-dashed line represent $\beta = 1$ and 0.1, respectively.

$y^0_{\mathrm{NH_3}} = 0.1$. The black and red lines represent $\beta = 1$ and 0.1, respectively. The carbon concentration increases linearly with the input TMG ratio. This means that increasing TMG increases the partial pressure of CH_4 near the surface and thus the surface flux of adsorbed C, which leads to increasing carbon incorporation rate. Since carbon concentration is determined by (carbon incorporation rate)/(growth rate), this result shows that increment of carbon incorporation rate due to the increase of TMG is larger than that due to the growth rate. As mentioned above, carbon concentration increases with TMG in the experiments [7,8,11,13–15]. Thus, this calculated result agrees well with the measured trends. Furthermore, Fig. 3 shows that carbon concentration decreases with increasing total pressure (p_{total}). This tendency has also been reported in experiments [7,8]. These calculated results confirm the applicability and usefulness of the theoretical model. From the results for $\beta = 1$ (black line) and 0.1 (red dot-dashed line), i.e., $y_{\mathrm{Ga}} = y^0_{\mathrm{TMG}}$ and $y_{\mathrm{Ga}} = 0.1 \cdot y^0_{\mathrm{TMG}}$, we see that the carbon concentration is higher when $y_{\mathrm{Ga}} \ll y^0_{\mathrm{TMG}}$. This is because a lower Ga mole fraction near the surface with respect to the inlet flow leads to a lower growth rate while the C incorporation rate is almost constant. This result suggests that in order to decrease the carbon concentration in GaN, it might be effective to keep the Ga concentration high near the surface with respect to the CH_4 concentration by promoting the transport of Ga in the gas phase.

Figure 4 shows contours of carbon concentration when the input NH_3 mole fraction ($y^0_{\mathrm{NH_3}}$) and total pressure (p_{total}) are varied while keeping input TMG mole fraction constant: $y^0_{\mathrm{TMG}} = 10^{-4}$. Carbon concentration decreases with increasing input NH_3 mole fraction. This is because the surface N flux increases with NH_3 partial pressure. As a result, a Ga-exposed step edge which captures carbon atoms is immediately covered by nitrogen. Therefore, the carbon incorporation rate decreases with increasing NH_3 partial pressure. From

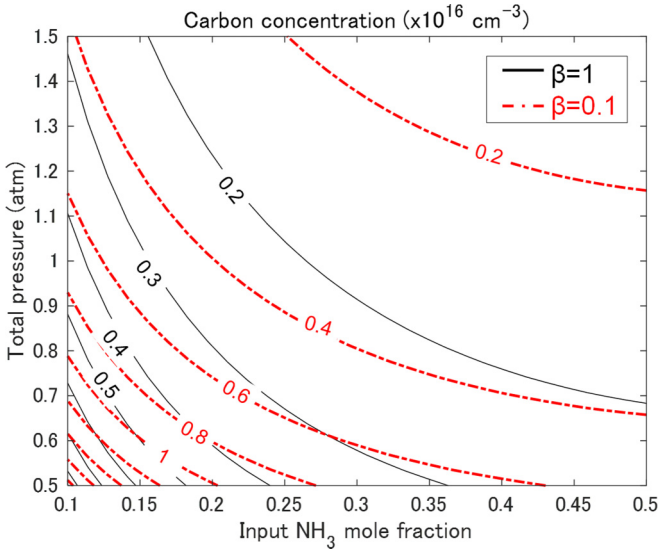

FIG. 4. Contour of carbon concentration as a function of input NH_3 ratio ($y^0_{NH_3}$) and total pressure (p_{total}). $T = 1000\,^\circ$C, $y^0_{TMG} = 10^{-4}$, $F = 10^{-5}$. Black line and red dot-dashed line represent $\beta = 1$ and 0.1, respectively.

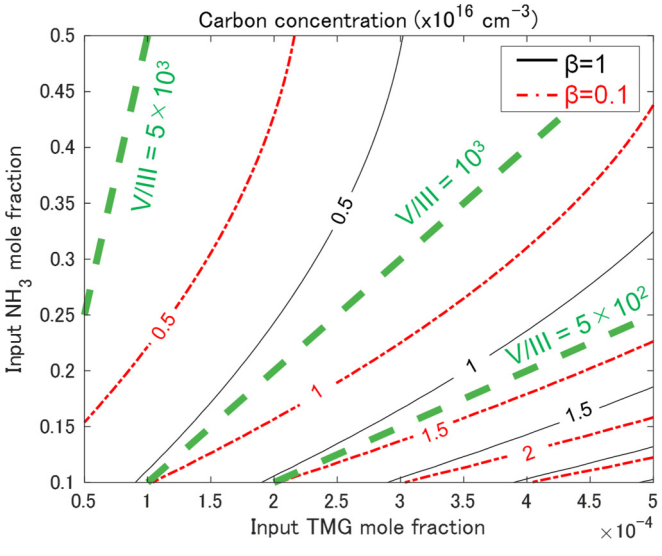

FIG. 5. Contour of carbon concentration as a function of input TMG ratio (y^0_{TMG}) and input NH_3 ratio ($y^0_{NH_3}$). $T = 1000\,^\circ$C, $p_{total} = 0.8$ atm, $F = 10^{-5}$. Black line and red dot-dashed line represent $\beta = 1$ and 0.1, respectively. Green dashed lines represent constant V/III ratio.

Eq. (17), carbon concentration decreases inverse proportionally to surface N flux, and from Eq. (29), surface N flux is proportional to NH_3 partial pressure near the surface. Therefore, carbon concentration is inversely proportional to NH_3 partial pressure near the surface, so that the carbon concentration is predicted to decrease as the NH_3 partial pressure increases, which is consistent with the experiments [7,8,10,12–16].

Figure 5 shows the contour of carbon concentration when the input NH_3 mole fraction ($y^0_{NH_3}$) and input TMG mole fraction (y^0_{TMG}) are varied while keeping total pressure constant at $p_{total} = 0.8$ atm. On green dashed lines in the figure, the V/III ratio ($=y^0_{NH_3}/y^0_{TMG}$) is constant at 5.0×10^2, 10^3, and 5.0×10^3, respectively. As seen in Figs. 3 and 4, carbon concentration decreases with decrease (increase) of TMG mole fraction (NH_3 mole fraction). Moreover, carbon concentration evidently stays almost constant under constant V/III ratio (see green dashed lines in Fig. 5). This result agrees with the experimental result of Piao *et al.* [14]. That is, the growth rate increases with increasing TMG at constant carbon concentration and constant V/III ratio. Furthermore, in the calculated results shown in Figs. 3–5, the carbon concentration is about $10^{15} \sim 10^{17}\,\mathrm{cm}^{-3}$, which is comparable to the typical value of carbon concentration measured experimentally. These calculational results appear to correctly predict carbon incorporation into GaN crystal during MOVPE. The proposed theoretical model can be expected to help control carbon impurities and thus to favor the development of high-voltage/high-current vertical GaN devices.

IV. CONCLUSIONS

In conclusion, we have proposed an impurity incorporation model for vapor phase epitaxy. Using this model, we investigated the relationships between carbon concentration in GaN grown by MOVPE and its growth conditions. In the proposed model, a kinetic growth process on crystal surface is considered. Carbon concentration was calculated based on thermodynamic properties and adsorption energies evaluated by first-principles calculations. The calculated results predict values of carbon concentration typical of those measured experimentally ($10^{15} \sim 10^{17}\,\mathrm{cm}^{-3}$). Furthermore, the calculated results also suggest that increasing input NH_3, increasing total pressure, and decreasing input TMG in MOVPE are effective ways to reduce carbon concentration, consistent with the reported experimental trends. The results of this study should be helpful in developing low carbon concentration GaN drift layers in high-voltage electronic devices.

ACKNOWLEDGMENTS

This work was partially supported by the JSPS KAKENHI Grant No. JP16H06418, MEXT GaN R&D Project, and JST CREST (Grant No. JPMJCR16N2).

[1] A. Tanaka, W. Choi, R. Chen, and S. A. Dayeh, Adv. Mater. **29**, 1702557 (2017).
[2] C. Gupta, Y. Enatsu, G. Gupta, S. Keller, and U. K. Mishra, Phys. Status Solidi A **213**, 878 (2016).
[3] I. C. Kizilyalli, P. Bui-Quang, D. Disney, H. Bhatia, and O. Aktas, Microelectron. Reliab. **55**, 1654 (2015).
[4] R. Li, Y. Cao, M. Chen, and R. Chu, IEEE Electron Device Lett. **37**, 1466 (2016).
[5] Y. Zhang, A. Dadgar, and T. Palacios, J. Phys. D **51**, 273001 (2018).
[6] T. Kachi, Jpn. J. Appl. Phys. **53**, 100210 (2014).

[7] D. D. Koleske, A. E. Wickenden, R. L. Henry, and M. E. Twigg, J. Cryst. Growth **242**, 55 (2002).
[8] N. A. Fichtenbaum, T. E. Mates, S. Keller, S. P. DenBaars, and U. K. Mishra, J. Cryst. Growth **310**, 1124 (2008).
[9] T.-T. Yuan, P.-Y. Kuei, L.-Z. Hsieh, T.-C. Li, and W.-J. Lin, J. Cryst. Growth **312**, 2239 (2010).
[10] J.-L. Zhang, J.-L. Liu, Y. Pu, W.-Q. Fang, M. Zhang, and F.-Y. Jiang, Chin. Phys. Lett. **31**, 037102 (2014).
[11] Q. Mao, J. Liu, X. Wu, J. Zhang, C. Xiong, C. Mo, M. Zhang, and F. Jiang, J. Semicond. **36**, 093003 (2015).
[12] F. Kaess, S. Mita, J. Xie, P. Reddy, A. Klump, L. H. Hernandez-Balderrama, S. Washiyama, A. Franke, R. Kirste, A. Hoffmann, R. Collazo, and Z. Sitar, J. Appl. Phys. **120**, 105701 (2016).
[13] W. V. Lundin, A. V. Sakharov, E. E. Zavarin, D. Y. Kazantsev, B. Y. Ber, M. A. Yagovkina, P. N. Brunkov, and A. F. Tsatsulnikov, J. Cryst. Growth **449**, 108 (2016).
[14] G. Piao, K. Ikenaga, Y. Yano, H. Tokunaga, A. Mishima, Y. Ban, T. Tabuchi, and K. Matsumoto, J. Cryst. Growth **456**, 137 (2016).
[15] O. I. Barry, A. Tanaka, K. Nagamatsu, S.-Y. Bae, K. Lekhal, J. Matsushita, M. Deki, S. Nitta, Y. Honda, and H. Amano, J. Cryst. Growth **468**, 552 (2017).
[16] T. Tanikawa, S. Kuboya, and T. Matsuoka, Phys. Status Solidi B **254**, 1600751 (2017).
[17] J. L. Lyons, A. Janotti, and C. G. Van de Walle, Phys. Rev. B **89**, 035204 (2014).
[18] M. Matsubara and E. Bellotti, J. Appl. Phys. **121**, 195701 (2017).
[19] M. Matsubara and E. Bellotti, J. Appl. Phys. **121**, 195702 (2017).
[20] P. Reddy, S. Washiyama, F. Kaess, R. Kirste, S. Mita, R. Collazo, and Z. Sitar, J. Appl. Phys. **122**, 245702 (2017).
[21] P. Kempisty, Y. Kangawa, A. Kusaba, K. Shiraishi, S. Krukowski, M. Bockowski, K. Kakimoto, and H. Amano, Appl. Phys. Lett. **111**, 141602 (2017).
[22] M. D. Pashley, Phys. Rev. B **40**, 10481 (1989).
[23] I. Barin, *Thermochemical Data of Pure Substances*, 3rd ed. (VCH, Weinheim, 1995).
[24] B. Delley, J. Chem. Phys. **92**, 508 (1990).
[25] B. Delley, J. Chem. Phys. **113**, 7756 (2000).
[26] J. P. Perdew, K. Burke, and M. Ernzerhof, Phys. Rev. Lett. **77**, 3865 (1996).
[27] K. Shiraishi, J. Phys. Soc. Jpn. **59**, 3455 (1990).
[28] T. Yayama, Y. Kangawa, and K. Kakimoto, Jpn. J. Appl. Phys. **52**, 08JC02 (2013).
[29] A. Kusaba, Y. Kangawa, P. Kempisty, K. Shiraishi, K. Kakimoto, and A. Koukitu, Appl. Phys. Express **9**, 125601 (2016).